International Journal of GEOMATE
(Geotechnique, Construction Materials and Environment)
ISSN: 2186-2982 (P), 2186-2990 (O), Japan
Vol. 31, Issue 145, September 2026, PP.1-9; DOI: 10.21660/2026.145.5312

# MODELING OF 2020 LAND SUBSIDENCE IN NINH KIEU DISTRICT, VIETNAM: FINITE ELEMENT ANALYSIS AND INSAR COMPARISON

Tran The Viet[1], Pham Phu Vinh[2], Hoang Thi Lua[3], Than Van Van[4*], Nguyen Huu Hue[5], Giang Hoang Hiep[6]

[1,2,3,4,5]Thuyloi University, 175 Tay Son, Kim Lien, Hanoi, Vietnam
[6]Vietnam Institute of Meteorology, Hydrology and Climate Change, Vietnam

*Corresponding Author, Received: 27 Oct. 2025, Revised: 12 Mar. 2026, Accepted: 09 June 2026

**ABSTRACT:** Land subsidence is a significant environmental hazard in the Mekong Delta, driven by the combined effects of weak Holocene sediments, rapid urbanization, and intensive groundwater extraction. This study reconstructs the land subsidence pattern of 2020 in Ninh Kieu District, Can Tho City, using a finite element modeling approach. The model incorporates detailed soil stratigraphy, building and surface loads, and groundwater-induced pore pressure variations to simulate representative annual settlement under the hydrogeological and loading conditions of 2020. Results reveal substantial spatial variability, with simulated subsidence rates ranging from 10 to 35 mm/year, concentrated along major roads, reclaimed zones, and newly developed urban areas underlain by thick, soft clay deposits. InSAR-derived deformation data for 2015–2020 were utilized for qualitative comparison, demonstrating good spatial agreement with the simulated hotspots of deformation. The study illustrates the effectiveness of physics-based modeling for reconstructing subsidence in deltaic environments and provides a methodological foundation for future scenario-based assessments of land subsidence and urban resilience planning in the Mekong Delta.

*Keywords: Land Subsidence; Finite Element Modeling; InSAR Analysis; Groundwater Extraction; Mekong Delta*

## 1. INTRODUCTION

Land subsidence is a gradual but significant geohazard that is becoming increasingly apparent in many delta regions [1]. Once it begins, the process is irreversible, and its effects on buildings, farmland, and infrastructure often become evident only after considerable damage has taken place. Worldwide, especially in rapidly urbanizing areas that depend heavily on groundwater, subsidence has been recorded at alarming rates. In most cases, the primary cause is the overexploitation of aquifers [1-4].

The Mekong Delta (MD) is one of the most evident examples of this issue. The delta ranks among the largest and most densely populated in the world, yet much of its land lies less than one meter above sea level [5]. This already delicate environment is exacerbated by human activities. In Can Tho City, the primary economic center of the delta, the ground has been sinking by an average of 10–30 mm per year, with some areas experiencing more than 40 mm per year [6]. In contrast to the global average sea-level rise of only 3–4 mm per year, it is evident that the relative sea-level rise here is driven much more by subsidence than by the ocean itself [5, 7]. Districts like Ninh Kieu, where development is dense and water demand is high, are particularly at risk. The physical manifestations of these high subsidence rates are already visible in the local infrastructure, such as the detachment and tilting of pedestrian sidewalks from bridge abutments observed at sites like Cai Son Bridge.

Several factors contribute to the rapid sinking of the ground in the MD [7-10]. The most significant is intensive groundwater pumping, which has lowered groundwater levels and caused the compressible layers of clay and silt to compact. Studies indicate drawdowns of 0.3 – 0.5 m per year in certain urban areas, resulting in corresponding ground lowering of 10 – 25 mm annually [7, 11]. Urban growth has also added weight to the ground surface: new buildings, roads, and embankments have increased stress on already weak soils, accelerating settlement [12]. Additionally, the geological foundation of the delta is inherently weak, consisting of thick Holocene deposits that compress easily, even under relatively minor changes in pressure [6].

Understanding the physical parameters and consolidation characteristics of these soil layers is a key factor for accurate subsidence forecasting [14]. Recent investigations using Modified Constant Rate of Strain (MCRS) tests on soft clays have demonstrated that the stiffness modulus increases proportionally with vertical stress and strain rates [13]. Higher strain rates have been shown to result in smaller settlement and greater soil stiffness, highlighting the complex geomechanical response of the delta's subsurface [13]. Furthermore, the selection of appropriate soil constitutive models remains critical for numerical accuracy [15]. Comparative studies in similar deltaic environments suggest that the Hardening Soil model (HSM) is more capable of capturing the complex behavior of soft soils under fluctuating groundwater levels compared to the conventional Mohr-Coulomb model [15] Additionally, for highly compressible formations with significant time-dependent deformation, the Soft Soil Creep (SSC) model has been increasingly recognized for its ability to simulate long-term creep effects, which are particularly prevalent in the thick clay deposits of the Mekong Delta.

In recent years, technologies like InSAR have enhanced our ability to monitor how and where the land is sinking [7, 11]. Although PSInSAR is an effective technique for monitoring long-term subsidence, it still has several inherent limitations. Its accuracy is strongly dependent on the availability and spatial density of persistent scatterers, which limits its applicability in vegetated or sparsely built areas where such scatterers are scarce (1). Moreover, PSInSAR measurements are influenced by atmospheric disturbances (2) and are restricted to deformation components along the satellite line of sight. In addition, the use of long temporal datasets may lead to the accumulation of orbital, DEM, and residual atmospheric errors, which can introduce temporal drift in the derived deformation time series (2). Furthermore, because InSAR techniques average measurements over specific pixel areas, they tend to "smooth" out extreme localized values, which can lead to the underreporting of critical subsidence hotspots occurring at the scale of individual construction projects. However, predicting future conditions continues to be challenging [16]. Many existing studies have concentrated on hydrology or statistical trends, while fewer have integrated groundwater dynamics, soil stratigraphy, and construction loads within a numerical modeling framework [6]. Research from other regions, such as the subsidence-affected plains of Greece [2] demonstrates the value of combining geological and hydrological data with finite element simulations. Such integrated approaches remain uncommon in the Mekong Delta.

This study aims to reconstruct the land subsidence pattern in Ninh Kieu District, Can Tho City, for the year 2020, using a finite element modeling approach that incorporates detailed geotechnical, hydrogeological, and surface loading conditions. The model simulates settlement behavior under the representative loading and groundwater conditions of 2020, enabling a realistic assessment of spatial variability in deformation throughout the district. InSAR-derived deformation data from 2015 to 2020 are utilized for qualitative comparison to evaluate the spatial coherence between simulated and observed subsidence patterns. By integrating numerical modeling with remote sensing analysis, the study provides a physically grounded understanding of land subsidence mechanisms in deltaic urban environments and establishes a methodological foundation for future scenario-based assessments under changing groundwater and climate conditions.

## 2. RESEARCH SIGNIFICANCE

This study enhances current subsidence research in the Mekong Delta by integrating soil stratigraphy, groundwater dynamics, and urban loading within a Finite Element Modeling framework. The primary novelty lies in applying the SSC model to capture both consolidation and long-term creep within thick Holocene clay deposits. Unlike observation-based analyses, it reconstructs process-driven deformation patterns and identifies localized settlement hotspots exceeding 40–50 mm/year. InSAR-derived deformation data were utilized for qualitative comparison, reinforcing the spatial coherence of results. The approach offers new insights into subsidence mechanisms and supports practical applications in urban planning, groundwater management, and climate adaptation in deltaic environments.

## 3. STUDY AREA AND DATA USED

The present study is conducted within the framework of the scientific program entitled "Study on land subsidence serving flood prevention in Ho Chi Minh City and the Mekong Delta urban areas" (Project Code: ĐTĐL.CN-62/2) , managed by the Ministry of Science and Technology (MOST) of Vietnam.

### 3.1 Location of the Study Area

The study area, about 12 km² in the northeastern part of Ninh Kieu District (Con Khuong, Cai Khe, An Hoa, and Thoi Binh wards), represents the urban core of Can Tho City (Fig. 1). This district exemplifies the main drivers of land subsidence in the Mekong Delta, including rapid urbanization, intensive groundwater abstraction, weak Holocene sediments, and climate-related stressors. High population density and concentrated infrastructure impose significant loads on compressible clay deposits, while groundwater extraction accelerates the consolidation.

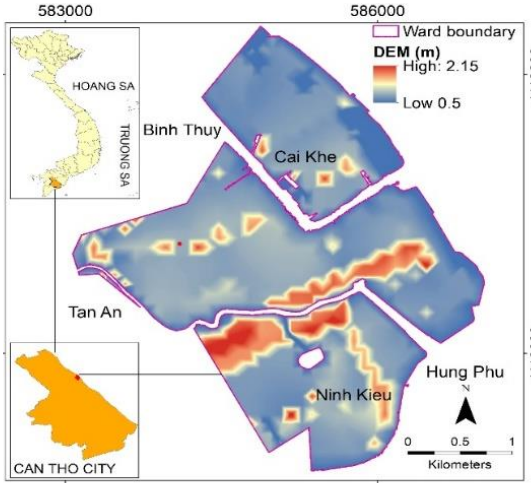


Fig.1 Location of the study area on the digital elevation background.

Figure 2 illustrates a typical case of land subsidence in the study area, observed at Cai Son Bridge on May 13, 2018. The pedestrian sidewalk has detached from the bridge abutment and tilted toward the roadway due to ground settlement, with visible displacement ranging from approximately 10 cm near the bridge structure to 25 cm at the outer edge of the sidewalk.


Fig. 2. View of Cai Son Bridge on May 13, 2018 [17]

### 3.2 Geological Conditions

For the numerical simulation, the study area was subdivided into 25 zones, as shown in Fig. 3. This division was implemented to address the challenges of spatial heterogeneity in geology, surface loading, and groundwater dynamics, which would otherwise require oversimplification in a single large-scale model and reduce reliability. By adopting this approach, model accuracy is enhanced, and computational limitations are effectively mitigated. Each zone was defined with relatively uniform soil stratigraphy and groundwater regimes, thereby allowing more representative boundary conditions and material parameters. The zone also prioritized areas with complex surface loading (e.g., infrastructure, roads) and sensitive zones affected by groundwater extraction or future development plans. Simulation results from all zones were later integrated to provide a detailed and reliable assessment of land subsidence across the entire study area.

According to the results of geotechnical drilling at several representative boreholes (Fig. 3) and the site investigation data, the subsurface conditions of the study area are characterized by highly heterogeneous soil stratification. The upper part of the profile consists of fill material with variable thickness (1.2 – 9.0 m), underlain by multiple interbedded soft to very soft clay layers (Layers 2, 4, 5) of high plasticity and large thickness variation, reaching up to 31.0 m.

Alternating with these weak soils are lenses of sandy silt and clayey sand (Layers 3, 5a), which are saturated and of low to medium density, further complicating the deposit. At greater depths, stiff to hard clays, sandy clays (Layers 6, 7, 8) occur, occasionally interbedded with thin lenses (Layer 8a). Below these, the deeper horizons consist of silty sand (Layer 9), which is medium dense and water-saturated, although not fully penetrated during drilling. Representative geological cross-sections between the boreholes in the study area are presented in Fig. 4.

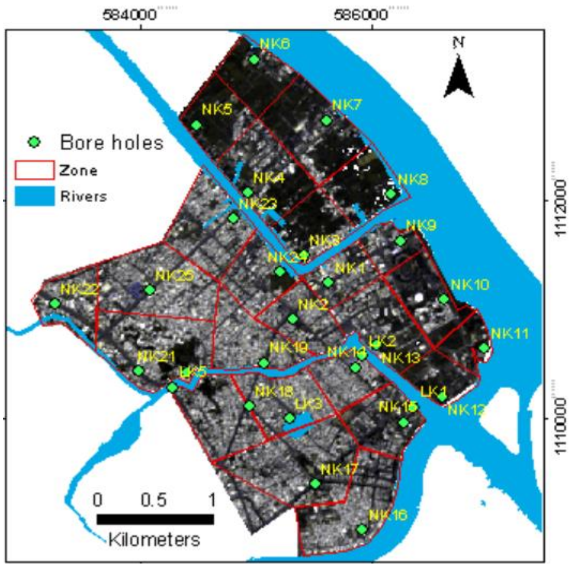


Fig.3 Zone map subdivided from the study area. Green points illustrate geological boreholes.

The characteristics of the subsoils in the study area were determined through a series of laboratory and in-situ tests carried out during the survey drilling program. Additional data were obtained from the regional geological association to complement the site investigation results. Table 1 summarizes the key physical and mechanical properties of the primary soil layers, which are then utilized for the settlement analysis discussed in the subsequent sections.

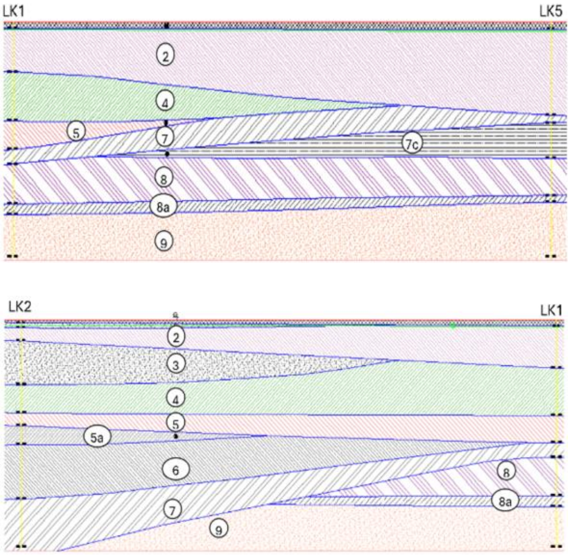


Fig.4. Representative geological cross sections of the study area.

### 3.3 Classification of Loads and Input Values

The distribution of loads illustrated in Fig. 5. As can be seen, the settlement modeling in Ninh Kieu District considers three main categories of loads: (i) structural loads, (ii) surface loads, and (iii) groundwater extraction–induced loads.

(i) Structural loads arise from residential, commercial, and industrial buildings, transmitted to the ground through foundations. Due to the weak Holocene sediments typical of the Mekong Delta, foundation types vary widely from shallow strip or raft foundations (often reinforced with timber piles) for low-rise houses, to reinforced concrete piles (driven or bored, 25–40 m in length) for mid- and high-rise buildings, and raft–pile or cement deep mixing solutions in riverside or very soft ground.

(ii) Surface loads include embankments, storage yards, industrial platforms, and road networks. These loads act directly on the ground surface and are treated as uniformly distributed pressures ranging from 10 to 40 kPa. Four representative categories were established: urban roads (15–25 kPa), storage yards for light materials (10–20 kPa), heavy-traffic or industrial yards (25–40 kPa). Short-term or highly localized loads were excluded, focusing instead on long-term, spatially significant effects.

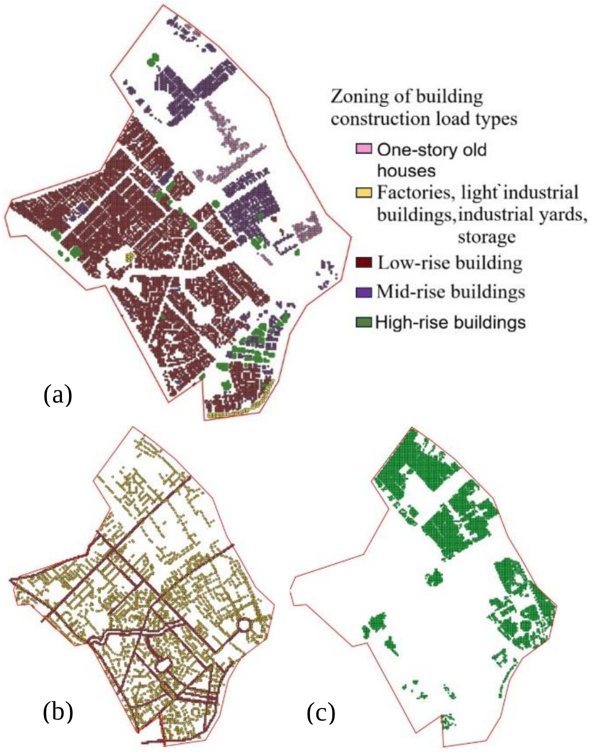


Fig.5 Current load zoning of the calculation area: (a) Zoning of structural loads, (b) Zoning of transportation loads, (c) Zoning of natural ground.

For the simulation, detailing each structure would necessitate extensive computational effort and highly specific investigation data; thus, six representative loading types, as summarized in Table 2, were adopted for the analysis. Average load pressures of 10–60 kPa were defined to capture typical loading conditions across the study area. The load history was examined to determine the representative settlement rate under the current conditions.

### 3.4 Selection of Soil Constitutive Models

The subsurface profile of the study area consists of sedimentary deposits extending to depths of 65–70 meters, with individual layers varying in thickness from 2 to 30 meters. Geotechnical data indicate that the upper 20–40 m is dominated by highly plastic clays (CH), characterized by high void ratios, low stiffness ($E_0 \approx$ 1,000–4,000 kPa), and significant compressibility, rendering them susceptible to large deformations under structural loading and groundwater fluctuations. Their settlement behavior is influenced by both primary consolidation and long-term creep.

Table 1. Physical and mechanical properties of the main soil layers in the study area.

| Description | Layers' notation | 2 | 3 | 4 | 5 | 6 | 7 | 8 | 9 |
|---|---|---|---|---|---|---|---|---|---|
| Properties | Unit | | | | | | | | |
| Soil classification | (-) | CH | SC | CH | CH | SC | CH | CL | SP |
| Total unit weight $\gamma$ | (kN/m³) | 15.50 | 17.9 | 16.28 | 16.77 | 18.84 | 19.3 | 17.20 | 18.30 |
| Dry unit weight $\gamma_d$ | kN/m³) | 9.61 | 12.9 | 10.99 | 11.67 | 14.3 | 14.9 | 15.21 | 15.30 |
| Initial void ratio *e* | (-) | 1.670 | 1.067 | 1.342 | 1.220 | 0.878 | 0.790 | 0.776 | 0.771 |
| Young modulus *E* | (kN/m²) | 1304.7 | 1935.0 | 2053.2 | 2571.2 | 7466.0 | 8465.0 | 13221.1 | 15152.1 |
| Effective cohesion *c*' | (kN/m²) | 6.57 | 7.7 | 17.36 | 12.56 | 7.5 | 31.88 | 26.01 | - |
| Effective friction angle $\varphi'$ | (degree) | 2.72 | 17.45 | 4.48 | 8.48 | 22.75 | 19.16 | 21.54 | 32.14 |
| Hydraulic conductivity k | (0.01 m/day) | 0.432 | 47.52 | 5.9616 | 0.342 | 7.0848 | 0.0849 | 0.06134 | 54.432 |
| Compression index *Cc* | (-) | 0.5581 | 0.1794 | 0.3022 | 0.2591 | - | - | - | - |
| Swelling index *Cs* | (-) | 0.0930 | 0.0299 | 0.0504 | 0.0432 | - | - | - | - |
| Creep index $C_\alpha$ | (-) | 0.005 | 0.0025 | 0.0035 | 0.0045 | - | - | - | - |

At greater depths, the deposits transition to denser silty sands (SC) and older clays, which are pre-consolidated under overburden pressure; these were represented by the Mohr–Coulomb (MC) model because of its simplicity, stability, and suitability for soils with predominantly elastic–plastic responses. The combined application of SSC for soft clays and Mohr–Coulomb for deeper, more competent strata provides a balanced framework that captures both time-dependent deformation in weak deposits and the mechanical resistance of stronger layers to ensure realistic ground behavior while maintaining computational efficiency. The main parameters for the material models of soil layers in the study area are presented in Table 1.

Figure 6 illustrates a representative cross-section under a particular loading condition of an arbitrary zone. Six models corresponding to the six foundation conditions will be simulated differently. In these models, soil layers 2, 3, and 4 are represented using the SSC model, while the other layers are modeled with the MC model.

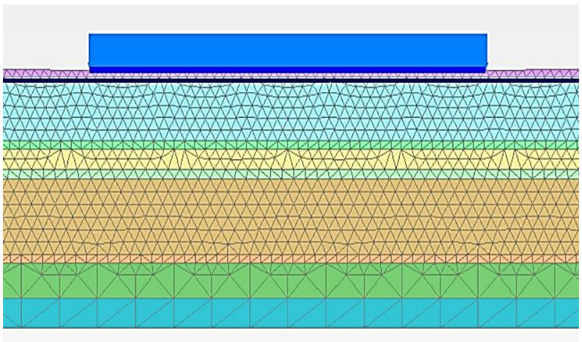

Fig. 6. Cross-section of an arbitrary zone

### 3.5 Settlement Due to Groundwater Extraction–Induced Loads

Groundwater extraction–induced loads represent a pseudo-load arising from the reduction in pore-water pressure when groundwater levels fall. Following Terzaghi's effective stress principle, a 1.0 m decline in groundwater level corresponds to an additional load of 9.8 kPa, which translates into increased effective stress. This load is approximately equivalent to that of a one-story building. This mechanism is especially significant in compressible clay layers, where consolidation and creep settlement can persist for decades.

Table 2 Classification of typical foundations and corresponding surface loads in Ninh Kieu, Can Tho

| Group notation | Type of structure | Design characteristics/ Typical description | Average load |
|---|---|---|---|
| MN1 | Low-rise houses | Shallow Foundations | 11 kPa |
| MN2 | Low-rise building | Timber piles, 3–6 m length, | 22 kPa |
| MN3 | Mid-rise buildings | Driven piles foundations, 15–25 m pile length | 33 kPa |
| MN4 | High-rise buildings | Pile foundations, 25–40 m pile length | 55 kPa |
| MN5 | Factories, light industrial buildings, Industrial yards, Storage yards, Containers | Raft foundation Raft thickness 0.5–1.0 m, | 18 kPa |
| MN6 | Urban roads | Transportation loads | 14 kPa |

To estimate land subsidence caused by groundwater drawdown, Plaxis includes a built-in feature that simulates fluctuations in groundwater levels over time. In this study, however, the settlement resulting from groundwater decline was evaluated analytically using a formula derived from Terzaghi's one-dimensional consolidation theory. The calculation method was selected for two main reasons. First, the soil layers within the groundwater extraction zone are relatively dense, located at considerable depths, and are only slightly affected by surface loading. Thus, it can be assumed that these layers exhibit nearly linear behavior within a small strain range and adhere to the one-dimensional consolidation theory when effective stress changes due to a uniform lowering of the groundwater level over a sub-area. Second, this approach helps to reduce modeling complexity in Plaxis, as combining multiple load scenarios with 25 calculation zones would otherwise result in a large number of computational models.

In this study, the rate of groundwater level decline per year across 25 sub-areas was examined. For the study area, the soil layers most impacted by the decline in the water column are mainly the two deepest layers, which act as confined aquifers and are characterized by relatively high permeability. Therefore, the dissipation of pore water pressure and the associated stress redistribution corresponding to the water head decline per year (ΔHw) are also assumed to be completed within one year. The resulting subsidence for one year (settlement rate) is estimated from the corresponding increase in effective stress in one year ($\Delta\sigma'_z = \Delta H_w \times \gamma_w$), using the following equations [18]:

+ For cohesive soil layers with compression index $C_c$:

$$\Delta H = \frac{C_C.H}{1+e_o} lg \frac{\sigma'_o + \Delta\sigma'_z}{\sigma'_o} \quad (1)$$

Where:

$\Delta H$ = settlement of the soil layer (m)

$H$ = initial thickness of the soil layer (m)

$e_0$ = initial void ratio (dimensionless)

$\sigma'_o$= initial average vertical effective stress (kPa)

+ For non-cohesive soil layers with Young modulus $E_o$:

$$\Delta H = \frac{\beta.\Delta\sigma'_z}{E_0} H \quad (2)$$

Where $\beta$ is calculated from the poisson's ratio $\boldsymbol{\mu_o}$ of the soil:

$$\beta = 1 - \frac{2\mu_o^2}{1-\mu_o} \quad (3)$$

### 3.6 Assignment of Model Results to Geographic Coordinates

For each of the 25 sub-zones, defined by specific groundwater level and geological conditions, numerical models were developed to simulate different loading scenarios. These scenarios were designed to represent the actual load distribution within each study sub-zone. This approach ensures that both geological characteristics and spatial variability in loads are adequately represented. Subsidence values at specific coordinates within the study area were then derived from the results of the cross-section corresponding to the load type acting at those locations. By mapping the numerical outputs back to their geographic positions, the model results can be spatially integrated, allowing the construction of settlement distribution maps that closely reflect the real conditions of Ninh Kieu Ward.

### 3.7 Development of Subsidence Rate Distribution Map

The regional settlement assessment was conducted using a multi-parameter integration framework. For each of the 25 geomechanical zones, settlement was simulated in Plaxis using zone-specific geological profiles. To account for structural variability, simulations were executed for all seven dominant foundation types, generating a comprehensive settlement matrix across time. To translate these discrete results into a regional scale, a 20 m × 20 m geospatial grid was superimposed over the Ninh Kieu District. The regional map was reconstructed through a spatial layer integration framework. For every grid node (x, y), a composite settlement value was calculated by identifying the intersection of four data layers: (1) geomechanical zone, (2) dominant construction/foundation type at that coordinate, (3) specific construction age, and (4) the localized groundwater drawdown rate. This integration allows for a high-resolution representation of spatial heterogeneity while maintaining the computational efficiency of the zoning approach.

## 4. RESULTS OF CURRENT SUBSIDENCE CONDITIONS (2020)

Following the methodology described in Section 3.7, the settlement rate across the study area was numerically simulated, and the corresponding results are illustrated in Fig. 7. As can be seen, the results show a clear spatial differentiation of subsidence rates across Ninh Kieu District. Most of the study area exhibits subsidence rates of 5–15 mm/year, particularly in An Hoa and Thoi Binh wards. Higher and more irregular subsidence occurs in Cái Khế and Con Khuong, where localized hotspots exceed 40 mm/year, while surrounding zones experience 20–30 mm/year. A notable pattern is the stronger subsidence along major roads compared to adjacent residential areas, forming linear subsidence strips likely caused by embankment loads and traffic-induced vibrations.

The most severe subsidence (>40 mm/year) corresponds to clusters of recently built temporary houses (2015–2020) with shallow foundations on weak clay, leading to rapid early-stage settlement. Moderate subsidence zones (20–25 mm/year) align with urban expansion areas developed in 2010–2020, where improved foundation design partly reduces differential settlement, though weak soils and groundwater extraction still sustain relatively high rates. In contrast, the southwest urban core, developed since the early 2000s, shows lower subsidence (10–15 mm/year), reflecting the completion of primary consolidation and only residual creep settlement.

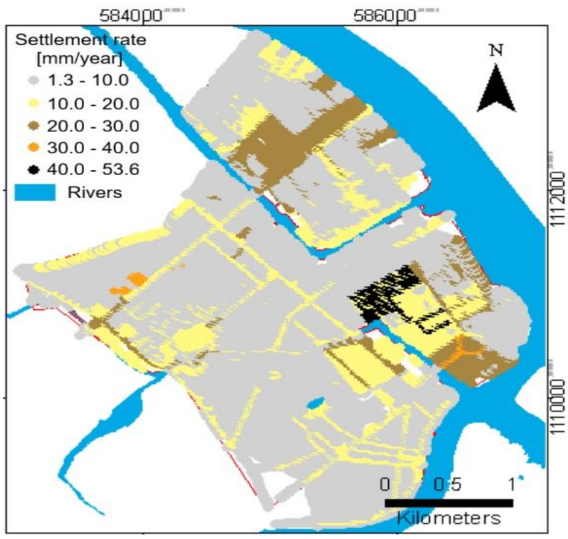


Fig. 7 Results showing the settlement rate of the study area

Overall, the 2020 results highlight a strong correlation between subsidence rates, urban development history, and foundation conditions. Hotspots appear in newly developed areas on weak ground, expansion zones sustain moderate settlement, while older built-up areas approach stabilization. These findings emphasize the importance of load management, groundwater control, and targeted ground improvement measures for sustainable urban development.

To evaluate the reliability of the simulated settlement rates, ground subsidence was independently estimated using the Persistent Scatterer Interferometric Synthetic Aperture Radar (PS-InSAR) technique. This analysis was based on a dataset comprising 140 Sentinel-1 SAR scenes acquired between July 2016 and December 2020. The resulting spatial distribution of settlement rates derived from this approach is illustrated in Fig. 8. While the current model is compared against regional InSAR data to verify displacement trends, it is noted that formal calibration against local leveling benchmarks or piezometric data remains an objective for future research as such data becomes available. The current comparison serves to demonstrate the model's capability in replicating regional geomechanical behavior.

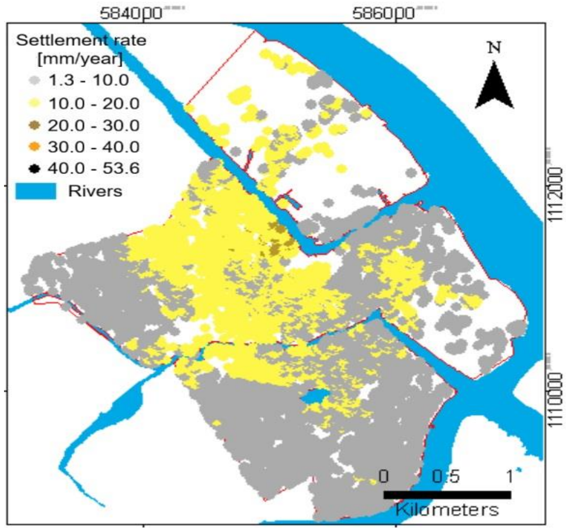


Fig. 8 Subsidence rates derived from InSAR analysis from 2015 to 2020

As can be seen, the analysis identified 20,618 subsiding points during this period. Most of the study area is experiencing subsidence at a rate of 3–5 mm/year, accounting for approximately 17% of all detected points. Central urban zones exhibit faster subsidence than peripheral areas, with the majority of points showing rates of 10 mm/year or higher. This spatial pattern is generally consistent with the modeling results, which also indicate greater subsidence in newly developed and densely built-up areas compared to older, more stabilized zones.

However, the numerical model indicates localized hotspots with subsidence rates of 40–50 mm/year, which are not distinctly identified by InSAR observations. This discrepancy can be explained by the model's sensitivity to weak soil conditions and newly applied structural loads, while InSAR measures average deformation over relatively large pixels, thereby smoothing out extreme local values.

To evaluate the accuracy of the simulated settlement results, a statistical validation was performed against observed InSAR data, the results are shown in Table 3. The validation yielded a Mean Absolute Error (MAE) of 6.42 mm/year and a Root Mean Square Error (RMSE) of 9.59 mm/year. While the median settlement values showed high agreement (8.80 mm/year for the simulated result vs. 8.12 mm/year for InSAR), the model exhibited a higher sensitivity to localized high-displacement zones compared to the satellite observations. A bias of -2.81 indicates that, on average, the InSAR rates are slightly lower than the model's predictions.

The scatterplot in Fig. 9 indicates a weak point-by-point correlation between the two datasets. This is likely due to differences in spatial resolution. Therefore, $R^2$ is not considered an informative metric for evaluating model performance and is not discussed further.

Table 3 Alignment and statistical validation of simulated results vs. InSAR measurements.

| Metric | Simulated result | InSAR measurement |
|---|---|---|
| Median Settlement | 8.8 mm/year | 8.12 mm/year |
| Mean Settlement | 11.18 mm/year | 8.36 mm/year |
| Max Settlement | 53.65 mm/year | 22.94 mm/year |
| Standard Deviation | 8.06 | 4.15 |
| Mean Bias (Mean Error) | | -2.81 mm/year |
| Mean Absolute Error (MAE) | | 6.42 mm/year |
| Root Mean Square Error (RMSE) | | 9.59 mm/year |

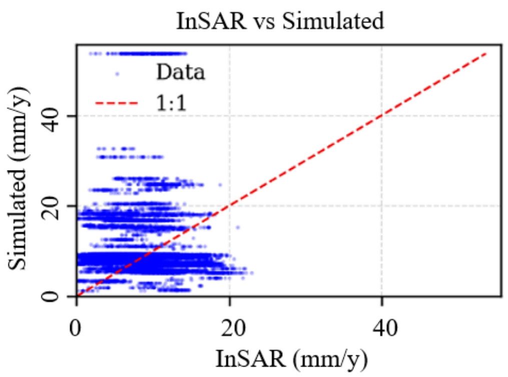


Fig. 9 Scatter plot of simulated settlement (FEM) versus observed InSAR measurements. The red dashed line represents the 1:1 perfect agreement.

Furthermore, a hotspot classification analysis was conducted using a threshold of 14.4 mm/year. The resulting confusion matrix demonstrated an overall classification accuracy of 69.4%, effectively identifying regional stability while highlighting areas where localized soil conditions and infrastructure development lead to accelerated subsidence.

The quantitative comparison reveals certain systematic differences between the simulated results and InSAR measurements, as evidenced by the mean bias of -2.81 mm/year and the spatial distribution of residuals. These discrepancies are primarily attributed to the differing spatial resolutions of the two methods. While the Finite Element Model (FEM) accounts for localized stress-strain variations based on specific borehole data - identifying hotspots of up to 53.65 mm/year - the InSAR measurements represent surface-level phase shifts averaged over a pixel area, which tend to 'smooth' extreme localized peaks. Despite these variations, the high agreement between median values (8.80 mm vs. 8.12 mm/year) confirms that the model accurately captures the primary geomechanical drivers of subsidence in the Ninh Kieu District.

## 5. CONCLUSION

This study reconstructed the 2020 land subsidence pattern in Ninh Kieu District, Can Tho City, through a physics-based finite element modeling framework that integrates soil stratigraphy, structural and surface loads, and groundwater-induced pore pressure variations. The results reveal pronounced spatial variability in subsidence rates—from less than 10 mm/year in stabilized areas to over 40 mm/year in newly developed zones underlain by thick soft clays and subjected to shallow foundations and intensive groundwater extraction.

Comparison with PS-InSAR deformation data from 2015–2020 indicates consistent spatial patterns between simulated and observed subsidence, particularly in identifying high-risk zones along major roads and recent urban expansion areas. Although differences in spatial resolution and temporal coverage limit direct point-by-point comparison, the combined analysis confirms that the numerical model captures the dominant subsidence mechanisms and effectively delineates localized deformation hotspots.

The findings provide practical insights for subsidence mitigation and urban planning in deltaic environments. High subsidence rates are closely linked to groundwater level decline, highlighting the importance of targeted groundwater management measures. In addition, the strong influence of foundation type suggests that deep pile foundations and ground improvement techniques should be prioritized for new construction in high-risk zones, while less intensive solutions may be suitable in areas where subsidence has stabilized.

Several limitations should be acknowledged. The numerical simulations rely on representative cross-sections within zoned areas and simplified assumptions regarding groundwater drawdown and consolidation behavior, which may not fully capture local three-dimensional interactions or short-term variability. In addition, InSAR-derived deformation represents multi-year averaged surface displacement, whereas the model simulates annual subsidence under representative conditions for 2020. Despite these limitations, the integrated modeling–InSAR framework provides a robust first-order assessment of subsidence processes and spatial risk patterns at the district scale.

Overall, this study demonstrates that finite element modeling, when combined with remote sensing observations, is an effective tool for linking observed land subsidence to underlying geotechnical and hydrogeological processes. The proposed framework can be readily extended to scenario-based analyses evaluating the impacts of groundwater management strategies, urban expansion, and climate-induced hydrological changes. With the support of integrated monitoring systems - combining InSAR, groundwater observations, GNSS, and geotechnical data - this approach can contribute to evidence-based planning and long-term resilience building for Can Tho City and other vulnerable urban areas in the Mekong Delta.

## 6. REFERENCES


1. Miranda A.T., Putranto D.D.A., Gunawan T.A. Flood and inundation risk analysis due to potential land subsidence on alluvial plains. International Journal of GEOMATE, 28(128), 2025, pp. 92-99.
2. Loupasakis C. An overview of the land subsidence phenomena occurring in Greece, triggered by the overexploitation of the aquifers for irrigation and mining purposes. Proceedings of the International Association of Hydrological Sciences, 382, 2020, pp. 321-326.
3. Artini S.R., Rosidawani, Putranto D.D.A. Land subsidence analysis in Palembang city using Differential Interferometric SAR. International Journal of GEOMATE, 28(129), 2025, pp. 105-112.
4. Saber M., Fattah M.A., Kantoush S.A., Sumi T. Implications of land subsidence due to groundwater over-pumping: monitoring methodology using grace data. International Journal of GEOMATE, 14(41), 2018, pp. 52-59.
5. Minderhoud P.S.J. The sinking mega-delta: present and future subsidence of the Vietnamese Mekong Delta, PhD Thesis, Utrecht University, Utrecht, 2019, pp. 1-200.
6. Minderhoud P.J.P., Coumou L.E., Erban L.E., Middelkoop H., Stouthamer E., Addink E.A. The relation between land use and subsidence in the Vietnamese Mekong delta. Science of The Total Environment, 634, 2018, pp. 715–726. https://doi.org/10.1016/j.scitotenv.2018.03.372
7. Erban L.E., Gorelick S.M., Zebker H.A. Groundwater extraction, land subsidence, and sea-level rise in the Mekong Delta, Vietnam. Environmental Research Letters, 9(8), 2014, pp. 1-6. Doi: 10.1088/1748-9326/9/8/084010
8. Anthony E., Brunier G., Besset M., Goichot P., Dussouillez P., Nguyen V.L. Linking rapid erosion of the Mekong River delta to human activities. Scientific Reports, 5(14745), 2015, pp. 1-12. https://doi.org/10.1038/srep14745
9. de Wit K., Lexmond B.R., Stouthamer E., Neussner O., Dörr N., Schenk A., Minderhoud P.S.J. Identifying Causes of Urban Differential Subsidence in the Vietnamese Mekong Delta by Combining InSAR and Field Observations. Remote Sensing, 13(189), 2021, pp. 1-33. https://doi.org/10.3390/rs13020189
10. Takagi H., Thao N.D., Anh L.T. Sea-Level Rise and Land Subsidence: Impacts on Flood Projections for the Mekong Delta’s Largest City. Sustainability, 8(959), 2016, pp. 1-15.
11. Tran V.T, Huynh V.T.M, Ram A., Pankaj K., Huynh V., Massaki K. Spatiotemporal variations in groundwater levels and the impact on land subsidence in CanTho, Vietnam. Groundwater for Sustainable Development, 15, 2021, pp. 1-13.
12. Tran V.T, Nguyen T.T, Nguyen V.A.M, Nguyen T.T. Evaluating the impacts of groundwater extraction on land subsidence in Cai Rang district, Can Tho City. Journal of Materials and Construction, 11(1), 2021, pp. 25-31..
13. Tran T.V, Pham H.D. Effect of strain rate on consolidation characteristics of artificial silty clay: insights from modified constant rate of strain tests. International Journal of GEOMATE, 27(124), 2024, pp. 87–94. https://doi.org/10.21660/2024.124.4705
14. Nguyen V.A.M, Thongchart S., Mairaing W. Roadway settlement characteristics on mekong delta for various landforms. International Journal of GEOMATE, 25(111), 2023, pp. 83–93.
15. Intui S., Namjan T., Kosinanondh N., Chaiprakaikeow S., Inazumi S. The impact of soil constitutive model selection on ground surface settlement analysis. International Journal of GEOMATE, 29(133), 2025, pp. 47–54.
16. Collados-Lara A., Pulido-Velazquez D., Mateos R., Ezquerro P. Potential impacts of future climate change scenarios on ground subsidence. Water, 12(219), 2020, pp. 1-16.
17. Neussner O. Trouble Underground - Land Subsidence in the Mekong Delta. Research report, Registered offices Bonn and Eschborn, Germany, 2019, pp. 1-62.
18. Terzaghi K., Peck R.B., Mesri G. Soil mechanics in engineering practice, John Wiley and Sons, Hoboken, NJ, USA, 1996, pp. 1–592.